Geomechanics and Engineering, *Vol. 42, No. 6 (2025) 463-473*
https://doi.org/10.12989/gae.2025.42.6.463

Effects of cyclic frequency on the dynamic response and liquefaction resistance of silica sands with different grain size distributions

Dong-Kiem-Lam Tran*[1] and Sung-Sik Park**[2]

[1]*Department of Civil Engineering, University of Architecture Ho Chi Minh City, Ho Chi Minh City, Viet Nam*
[2]*Department of Civil Engineering, Kyungpook National University, 80, Daehak-ro Buk-gu, Daegu 41566, Republic of Korea*

(*Received July 1, 2025, Revised September 18, 2025, Accepted September 22, 2025*)

Abstract. This study investigates the effect of loading frequency on the liquefaction resistance of reconstituted sandy soils with different grain size distributions. Three sand samples (SAND1, SAND2, and SAND3) were tested under undrained cyclic loading using the cyclic direct simple shear (CDSS) test. The experimental program was performed at multiple cyclic stress ratios (*CSRs*) and loading frequencies ranging from 0.03 Hz to 0.5 Hz. The number of cycles to liquefaction ($N_{cyc\text{-}liq}$), excess pore water pressure generation, and cyclic resistance ratio at 15 cycles (CRR_{15}) were evaluated to assess the frequency-dependent liquefaction behavior. The results reveal a consistent trend across all three sand types, characterized by two distinct behavioral zones. In the low-frequency range (0.03–0.10 Hz), the influence of frequency on $N_{cyc\text{-}liq}$ and CRR_{15} is minimal. However, when the frequency exceeds 0.10 Hz, both parameters exhibit significant increases, indicating enhanced liquefaction resistance. This transition at 0.10 Hz was observed consistently, regardless of CSR level or soil type, and is proposed as a threshold frequency distinguishing a Stable/Minor-Effect Zone from an Increasing Resistance Zone. The findings underscore the importance of incorporating loading frequency into liquefaction assessments. The threshold frequency offers a useful reference for engineering calculations and seismic stability assessments of sandy soils, as it marks the boundary beyond which frequency effects must be carefully considered in liquefaction evaluation and design.

Keywords: cyclic direct simple shear test; liquefaction resistance of sand; loading frequency

1. Introduction

The ongoing expansion of urban areas and the increasing number of civil, industrial, and infrastructure projects in seismically active zones have emphasized the need for a clear understanding of how saturated soils respond to cyclic and seismic loading. Among the potential hazards associated with such loading conditions, soil liquefaction remains one of the most critical concerns. This phenomenon occurs when excess pore water pressure builds up during repeated shearing, leading to a reduction—sometimes complete loss—of effective stress (NRC 1985, Boulanger and Idriss 2006). As a result, the soil loses its shear strength, potentially causing severe damage to foundations and supporting ground structures (Youd *et al.* 2001).

Historic earthquakes such as the 1964 Niigata Earthquake in Japan (Bhattacharya et al. 2014) and the 1964 Alaska Earthquake in the USA (Coulter and Migliaccio 1966) provided early and compelling evidence of the destructive consequences of liquefaction in saturated sandy soils. These events sparked intense research efforts and positioned liquefaction as a fundamental issue in soil dynamics and geotechnical earthquake engineering.

The resistance of soil to liquefaction and its dynamic behavior are influenced by a wide range of factors. These include soil-related parameters such as density, void ratio (Vaid and Sivathayalan 2000, Kokusho 2007), fines content (Park and Kim 2013, Zuo *et al*. 2023, Park *et al*. 2024), and particle size distribution (Chang and Ko 1982, Vaid *et al.* 1990, Sonmezer *et al.* 2020); loading characteristics such as cyclic stress ratio, shear strain amplitude, initial static shear stress, and loading frequency (Dash and Sitharam 2016, Park *et al.* 2023); and testing conditions, including specimen dimensions, confinement method, and preparation technique (Amipour *et al.* 2022, Tran *et al*. 2024a, Park and Lee 2024).

While significant progress has been made in understanding the roles of fines content, relative density, and initial static shear stress, the effect of cyclic loading frequency has not been as extensively explored. The influence of loading frequency on the liquefaction resistance of sands has been widely investigated, but the results remain inconsistent and, in some cases, contradictory. While many studies have reported a positive correlation between loading frequency and liquefaction resistance, others have observed negligible or even inverse effects.

Several experimental studies have demonstrated that an increase in loading frequency tends to enhance the liquefaction resistance of sands. This trend is commonly reflected by an increase in the number of cycles required to trigger liquefaction ($N_{cyc\text{-}liq}$) and a corresponding increase in cyclic resistance ratio (Lee and Fitton 1969, Chang *et al.*

*Corresponding author, Ph.D.
E-mail: lam.trandongkiem@uah.edu.vn
**Corresponding author, Ph.D
E-mail: sungpark@knu.ac.kr

ISSN: 2005-307X (Print), 2092-6219 (Online)

1982, Zhu *et al*. 2021, Yue *et al.* 2023). For example, in saturated Monterey No. 0 sand, it was found that the frequency effect became significant when the loading frequency exceeded 0.01 Hz, and the effect intensified with increasing frequency (Chang *et al.* 1982). In cyclic direct simple shear (CDSS) tests on Nakdong River sand, increasing the frequency from 0.05 Hz to 0.1, 0.5, and 1 Hz led to improvements in liquefaction resistance by approximately 3.7%, 7.9%, and 12% for loose sands, and 2.9% and 19% for dense sands (Nong *et al*. 2020). Similarly, for saturated Fujian sand, the CRR_{15} value increased by about 25% when the loading frequency rose from 0.05 Hz to 2 Hz (Yue *et al*. 2023). Comparable behavior was observed in coral sands, where higher frequencies resulted in improved liquefaction resistance (Qin 2023, Zhou 2025).

In contrast, several studies have concluded that loading frequency exerts little or no influence on the liquefaction resistance of saturated sands (Peacock and Seed 1968, Yoshimi and Oh-oka 1975, Vernese and Lee 1977, Tatsuoka *et al*. 1983, Hussain and Sachan 2019). For instance, experiments on Bandaijima sand across a frequency range from 1 Hz to 12 Hz showed that liquefaction triggering conditions were essentially independent of loading frequency (Yoshimi and Oh-oka 1975). Similar results have been reported for various sand, where the frequency effect was minimal or statistically insignificant (Wong *et al.* 1975, Lee and Focht 1975, Tatsuoka *et al*. 1986, Hussain and Sachan 2019).

Interestingly, a number of studies have even observed a reverse trend, where liquefaction resistance decreased with increasing loading frequency. Mulilis *et al*. (1975) found that Monterey sand tested at a low frequency of 0.017 Hz exhibited approximately 20% greater liquefaction resistance compared to the same sand tested at 1 Hz. Dash and Sitharam (2016) reported similar findings for Ahmedabad sand, where liquefaction resistance decreased with increasing frequency, suggesting that lower frequencies may enhance soil stability under cyclic loading.

Moreover, previous studies on this topic often report contradictory results (Park *et al*. 2023), suggesting that the relationship between loading frequency and liquefaction behavior is complex and not yet fully understood. This gap highlights the importance of further investigation into how frequency influences pore pressure generation, shear deformation, and the number of cycles to liquefaction under different soil conditions.

In the present study, a comprehensive series of stress-controlled cyclic direct simple shear (CDSS) tests was performed on different soil types to systematically evaluate the influence of loading frequency on the variation of excess pore pressure development, and liquefaction resistance.

2. Material and testing program

2.1 Soil properties

Three different types of sand, denoted as SAND1, SAND2, and SAND3, were selected for the experimental investigation based on their distinct particle size distributions, as illustrated in Figure 1. These soils were chosen to represent a range of gradation characteristics, from poorly graded to well-graded sands. The fundamental grain-size parameters, including the effective diameters (D_{10}, D_{30}, D_{50}, D_{60}), the coefficient of uniformity (C_U), and the coefficient of gradation (C_g), are summarized in Table 1.

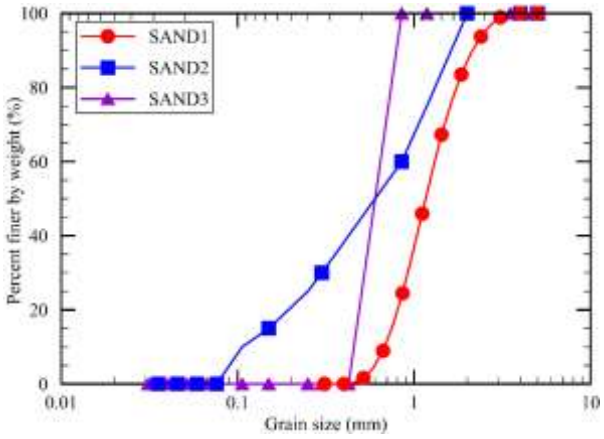

Fig. 1 The particle size distribution curve of testing material

Table 1 Basic grain-size parameters of the tested sands

Type	D_{10} *(mm)*	D_{30} *(mm)*	D_{50} *(mm)*	D_{60} *(mm)*	C_u	C_g
SAND1	0.678	0.921	1.165	1.310	1.93	0.95
SAND2	0.106	0.300	0.638	0.850	8.02	1.00
SAND3	0.468	0.553	0.638	0.680	1.45	0.96

SAND1 represents a relatively coarse and poorly graded material with low uniformity, while SAND2 exhibits characteristics of a well-graded fine sand. SAND3 presents an intermediate gradation profile with moderate sorting. These differences in gradation are expected to influence the cyclic behavior and liquefaction resistance under varying loading frequencies.

2.2 Cyclic Direct Simple Shear (CDSS) test

The Cyclic Direct Simple Shear (CDSS) test is a laboratory-based geotechnical testing method widely employed to investigate the cyclic behavior of soils under earthquake-induced loading conditions. The CDSS testing presents several distinct advantages that make it a preferred method in geotechnical earthquake engineering. Firstly, it effectively replicates in-situ seismic conditions by applying repeated cyclic shear stresses or shear strains to the soil specimen, thereby closely simulating the loading experienced by soil elements during actual seismic events (Peacock and Seed 1968, Asadzadeh and Soroush 2017, Mohtar *et al.* 2018). Secondly, the CDSS test accommodates plane-strain deformation and principal stress rotation—critical aspects of soil behavior under real earthquake loading—which are difficult to achieve using conventional triaxial testing methods (Dyvik *et al.* 1987, Asadzadeh and Soroush 2017). Additionally, this testing

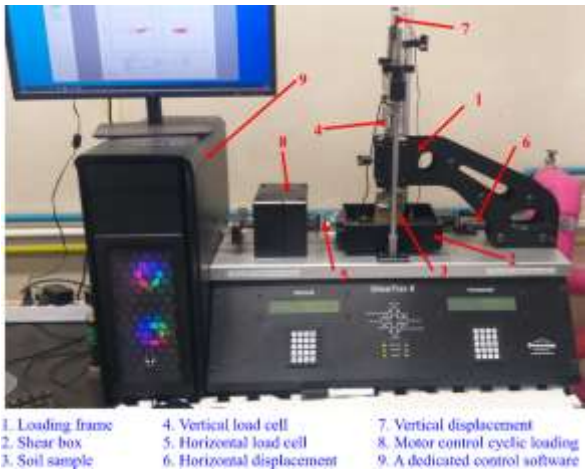

Fig. 2 The CDSS ShearTrac-II system

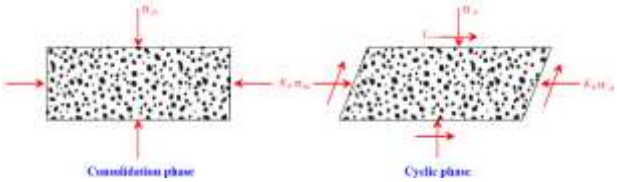

Fig. 3 Two phase of a typical CDSS test

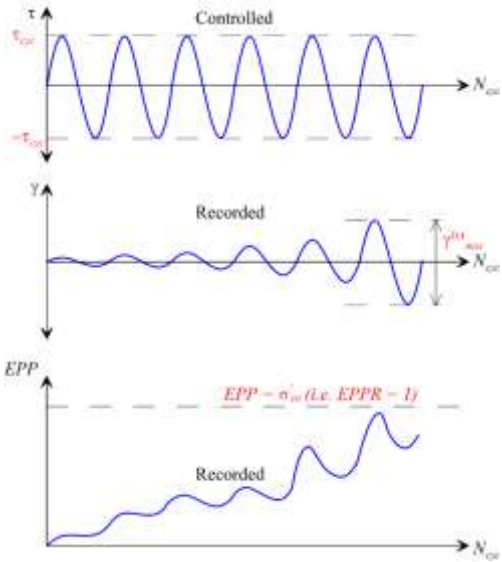

Fig. 4 Time series data of cyclic shear stress, shear strain, and EPP during an undrained stress controlled cyclic loading

method allows for direct monitoring of key parameters such as excess pore pressure generation, shear strain accumulation, and liquefaction resistance, providing valuable insights into the cyclic behavior of soils (Park *et al*. 2024, Tran *et al*. 2024a). From a geotechnical modeling standpoint, CDSS is particularly well-suited for representing the simple shear zones beneath foundations, which are prone to failure during seismic events, thus complementing the stress conditions modeled in compression and extension zones by other types of laboratory tests (Doherty and Fahey 2011).

The experimental program in this study was carried out using the ShearTrac-II cyclic simple shear system, a specialized apparatus developed by the Norwegian Geotechnical Institute (NGI) and manufactured by Geocomp Corporation (USA). This system is widely utilized in geotechnical research due to its high precision in controlling cyclic loading paths and its suitability for investigating soil liquefaction behavior under seismic loading conditions (Nong *et al*. 2021, Tran *et al*. 2024a, b).

The ShearTrac-II system comprises several key components, including a robust cyclic direct simple shear (CDSS) loading frame, a shear box, and both vertical and horizontal actuators that apply controlled stress to the soil specimen. The system is equipped with load cells and displacement transducers to accurately measure the applied forces and resulting deformations. A computer interface with dedicated control software enables the execution of either stress-controlled or strain-controlled test protocols, ensuring flexibility and accuracy in simulating field loading scenarios (Fig. 2).

2.3 Testing program and liquefaction criteria

For each test, a cylindrical soil specimen with a diameter of 63.5 mm and a height of 25 mm was carefully prepared and enclosed within a wire-reinforced membrane to maintain boundary conditions. In this study, soil specimens were prepared using the dry deposition method, a widely adopted technique in geotechnical laboratory testing to ensure uniformity and control over relative density. The preparation process involved the use of a narrow-spout funnel, with the tip of the spout initially positioned at the base of the specimen mold. Dry sand was gradually poured through the funnel while the funnel was slowly raised along the central vertical axis of the mold. This controlled pouring technique minimizes the free-fall height of the soil particles, thereby reducing particle segregation and enhancing control over the resulting specimen density. The dry deposition method is particularly effective in producing specimens with high vertical uniformity, mitigating the risk of stratification between coarse and fine particles, such as sand and silt (Wood *et al*. 2008, Yamamuro and Monkul 2010).

During the specimen preparation, the sand sample was enclosed in a reinforced rubber membrane to prevent lateral deformation, ensuring that consolidation proceeded under K0 conditions (i.e., zero lateral strain) (ASTM D8296 2019, Tran *et al.* 2024a). An initial vertical effective stress (σ'_{v0}) of 100 kPa was applied and maintained until the specimen reached a final deformation with a target relative density of 50%. This step ensured that the sample structure and density were representative of field conditions prior to seismic loading.

Upon completion of consolidation, the specimen was subjected to cyclic shear stress (τ_{cyc}) applied in the horizontal direction (Fig. 3).

The tests were conducted under stress-controlled conditions, with the cyclic loading frequencies set at 0.03, 0.05, 0.1, 0.2, and 0.5 Hz to evaluate strain accumulation and pore pressure generation across a range of seismic

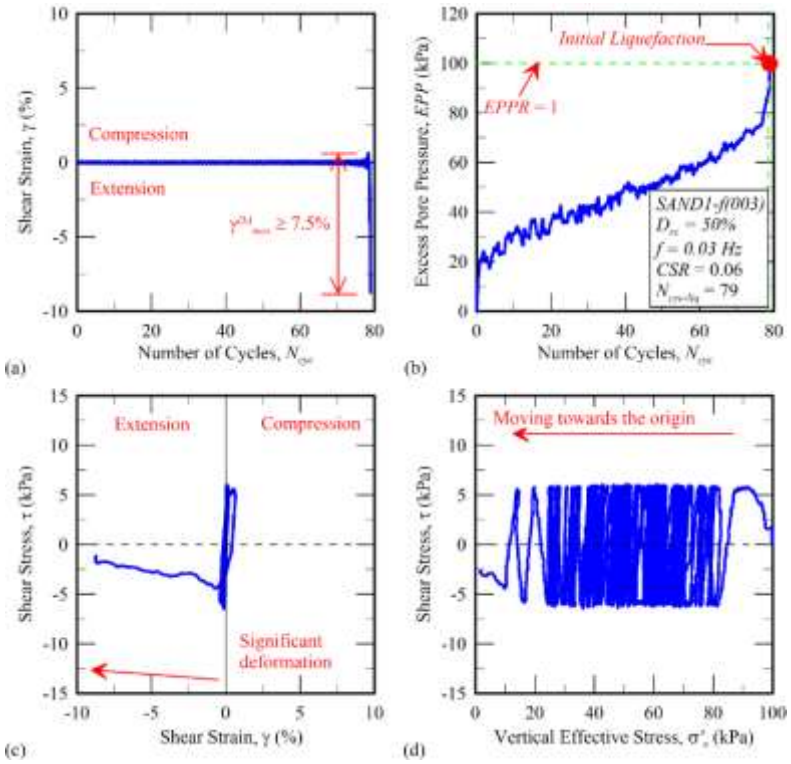

Fig. 5 The CDSS stress-controlled test result of sample ID SAND1-f(0.03), CSR of 0.06 at loading frequency of 0.03 Hz, relationship between: (a) shear strain and number of cycles, (b) excess pore pressure and number of cycles, (c) shear stress and shear strain, and (d) shear stress and vertical effective stress

loading rates. During this phase, the test was performed under constant-volume control to simulate undrained conditions, which are typical during short-duration seismic events. The excess pore pressure (*EPP*) developed during cyclic loading was inferred from changes in the vertical effective stress. Liquefaction triggering was defined based on one of two criteria: (i) when the excess pore pressure ratio reached 100% (i.e., complete loss of effective stress), or (ii) when the double amplitude shear strain ($\gamma^{DA}{}_{max}$) exceeded 7.5%, whichever occurred first (NRC 1985) (Fig. 4).

The detailed parameters of the cyclic direct simple shear tests are presented in Table 2, which summarizes the testing conditions such as soil type, loading frequency, cyclic stress ratio ($CSR = \tau_{cyc}/\sigma'_{v0}$), number of cyclic to require liquefaction, and cyclic stress ratio at 15 cycles (CRR_{15} - an earthquake magnitude of 7.5 - (Seed 1979)).

3. Results and discussion

3.1 Test results

The detailed results of all CDSS tests are summarized in Table 2, including key parameters such as sand type, loading frequency, the number of cycles to liquefaction ($N_{cyc\text{-}liq}$), and the cyclic stress ratio at 15 cycles (CRR_{15}). To illustrate the typical cyclic behavior of the soil specimens, three representative test cases are presented in Figs. 5-7, corresponding to samples SAND1-f(0.03), SAND2-f(0.03), and SAND3-f(0.50), respectively.

As shown in Fig. 5(a), the shear strain gradually increases during the early loading cycles, reflecting small, stable oscillations. However, starting from around the 71st cycle, the strain amplitude increases significantly. At the 79th cycle, the double amplitude shear strain exceeds the threshold of 7.5%, indicating the onset of initial liquefaction according to the strain-based criterion. This marks the point where the soil undergoes a rapid transition to large, unstable deformation. Simultaneously, Fig. 6(b) displays the evolution of excess pore pressure (EPP) with the number of cycles. The EPP increases progressively and reaches a critical value at the 79th cycle, where the excess pore pressure equals the initial vertical effective stress (approximately 100 kPa), and the excess pore pressure ratio (*EPPR*) equals 1. This corresponds to the liquefaction point based on the pore pressure criterion. The consistency in identifying liquefaction using both strain and pore pressure indicators enhances the reliability of the test observations. The cyclic stress–strain behavior is shown in Fig. 6(c). During the initial cycles, the hysteresis loops are narrow and nearly symmetric, indicating near-linear behavior. As loading continues and deformation accumulates, the loops widen and become increasingly asymmetric. After liquefaction, the loops exhibit large excursions in both extension and compression, and the behavior becomes markedly nonlinear with clear evidence of strain softening and permanent deformation. In Fig. 6(d), the relationship between shear stress and vertical effective stress is presented. The stress path progressively migrates toward the origin as the effective stress diminishes due to the build-up

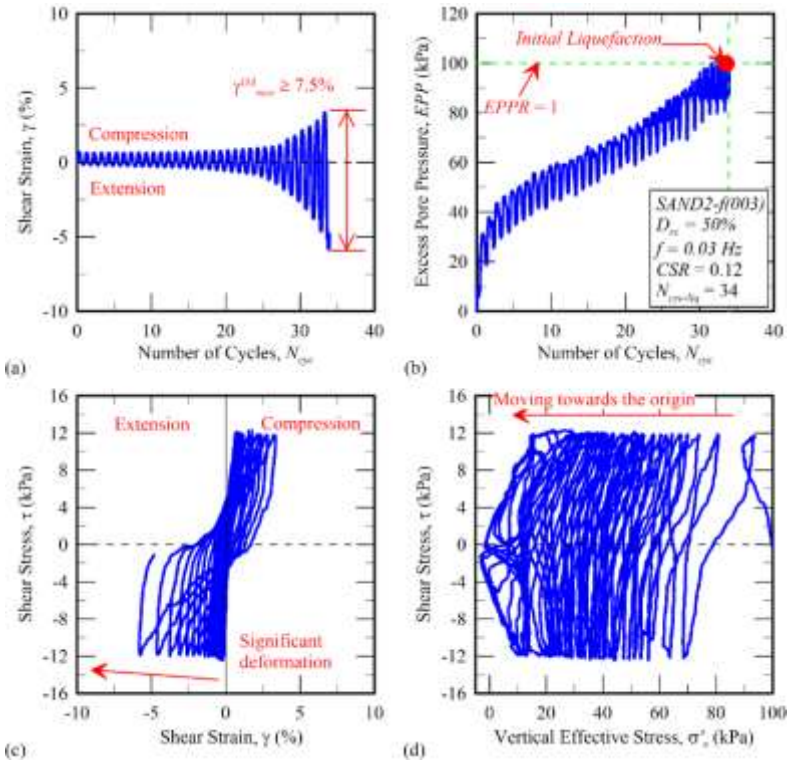

Fig. 6 The CDSS stress-controlled test result of sample ID SAND2-f(0.03), CSR of 0.12 at loading frequency of 0.03 Hz, relationship between: (a) shear strain and number of cycles, (b) excess pore pressure and number of cycles, (c) shear stress and shear strain, and (d) shear stress and vertical effective stress

Table 2 Summary of CDSS test results

IDs	*f*	*Number of cycles to cause liquefaction at CSRs of*					
	(Hz)	0.06	0.08	0.10	0.12	0.15	0.18
	0.03	79	17	6			
	0.05	77	16	8			
SAND1	0.10	81	19	7			
	0.20		52	12	2		
	0.50		72	44	13		
	0.03			102	34	12	
	0.05			100	33	13	
SAND2	0.10			101	39	14	
	0.20			110	55	18	5
	0.50			117	71	25	7
	0.03			70	31	10	
	0.05			71	34	13	
SAND3	0.10			70	35	13	
	0.20			77	51	14	
	0.50			111	66	18	5

of excess pore pressure. At the point of liquefaction, the effective stress approaches zero, and the stress path collapses, indicating the loss of intergranular contact and effective shear strength.

The other two samples, SAND2-f(0.03) and SAND3-f(0.50), shown in Figs. 6 and 7, exhibit similar trends with some distinctions. Sample SAND2-f(0.03), tested under a higher CSR (0.12) and frequency (0.03 Hz), reaches liquefaction earlier—after only 34 cycles—with a more rapid accumulation of strain and pore pressure. And the sample SAND3-f(0.50) was tested under frequency of 0.50, reaches liquefaction after 18 cycles. Despite these differences, all samples share the key features of cyclic degradation: progressive strain build-up, accumulation of excess pore pressure, eventual loss of effective stress, and pronounced changes in the shape and area of the hysteresis loops after liquefaction.

3.2 Effect of loading frequency on the excess pore pressure generation

The influence of loading frequency on the generation of excess pore pressure was investigated through a series of cyclic direct simple shear tests on sample SAND1 under two different cyclic stress ratios (CSR = 0.08 and 0.10). The results are presented in Fig. 8, where the excess pore pressure ratio is plotted against the number of loading cycles (N_{cyc}) for a range of loading frequencies: 0.03 Hz, 0.05 Hz, 0.10 Hz, 0.20 Hz, and 0.50 Hz.

Fig. 8(a) reveals a clear trend between loading frequency and the number of cycles required to trigger initial liquefaction ($N_{cyc\text{-}liq}$). At low frequencies (0.03 - 0.05 Hz), liquefaction occurs rapidly, with $N_{cyc\text{-}liq}$ ranging from 16 to 17 cycles, indicating fast and efficient accumulation of excess pore pressure. As the loading frequency increases to 0.10 Hz, a slight increase in $N_{cyc\text{-}liq}$ is observed, rising to 19 cycles. A more pronounced increase occurs at higher frequencies: 52 cycles for 0.20 Hz and 72 cycles for 0.50

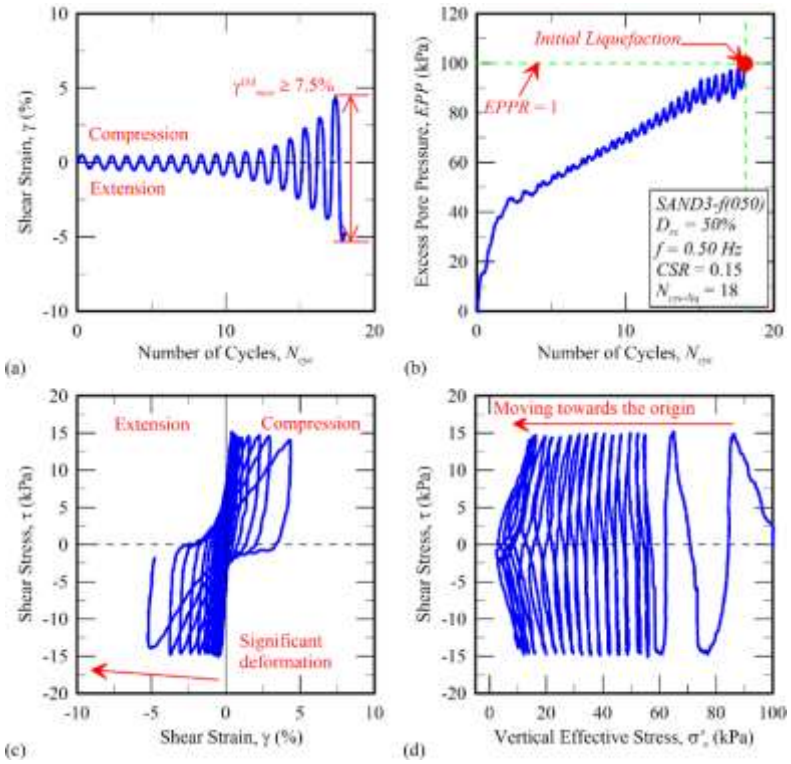

Fig. 7 The CDSS stress-controlled test result of sample ID SAND3-f(0.50), CSR of 0.15 at loading frequency of 0.50 Hz, relationship between: (a) shear strain and number of cycles, (b) excess pore pressure and number of cycles, (c) shear stress and shear strain, and (d) shear stress and vertical effective stress

Hz. This pattern suggests that at lower frequencies, the soil structure has more time per cycle to deform and mobilize pore pressure. Consequently, the build-up of excess pore pressure occurs quickly, and fewer cycles are needed to reach liquefaction. In contrast, at higher frequencies, the time interval between loading cycles is shorter, which may delay in the buildup of pore pressure due to incomplete pore pressure transfer. As a result, more cycles are required to accumulate sufficient pore pressure for liquefaction.

A similar trend is observed in Figure 8b, where the tests were repeated at a higher stress level (CSR = 0.10). In this case, liquefaction occurs more quickly overall due to the greater input energy per cycle. At low frequencies (0.03 - 0.05 Hz), the number of cycles to liquefaction is only 6 to 8, showing very rapid pore pressure accumulation. A minor increase to 7 cycles is seen at 0.10 Hz. As the frequency continues to rise, $N_{cyc\text{-}liq}$ increases to 12 cycles at 0.20 Hz and reaches 44 cycles at 0.50 Hz. Although the absolute values of $N_{cyc\text{-}liq}$ are lower compared to CSR = 0.08, the general frequency-dependent trend remains consistent: higher frequencies delay the onset of liquefaction by requiring more loading cycles to develop equivalent pore pressure levels. This confirms that the effect of loading frequency is independent of the CSR level and highlights its significant role in controlling the rate of pore pressure generation in sandy soils.

A similar trend can be observed in the SAND2 and SAND3 samples, as illustrated in Figs. 9 and 10, respectively. In both cases, the number of cycles required to trigger initial liquefaction increases significantly with

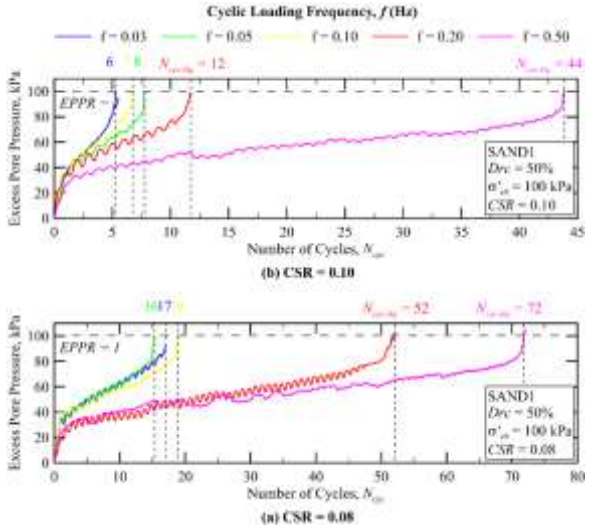

Fig. 8 Excess pore pressure generation versus number of cycles for the SAND1 sample under different loading frequencies: (a) CSR = 0.08 and (b) CSR = 0.10

higher loading frequencies, under the same applied CSR. This consistent pattern reinforces the observation that loading frequency plays a key role in controlling the rate of excess pore pressure accumulation and the onset of liquefaction.

To quantify the influence of loading frequency on the number of cycles to initial liquefaction under various CSR levels, Figure 11(a–c) presents the relationship between loading frequency and $N_{cyc\text{-}liq}$ for SAND1, SAND2, and

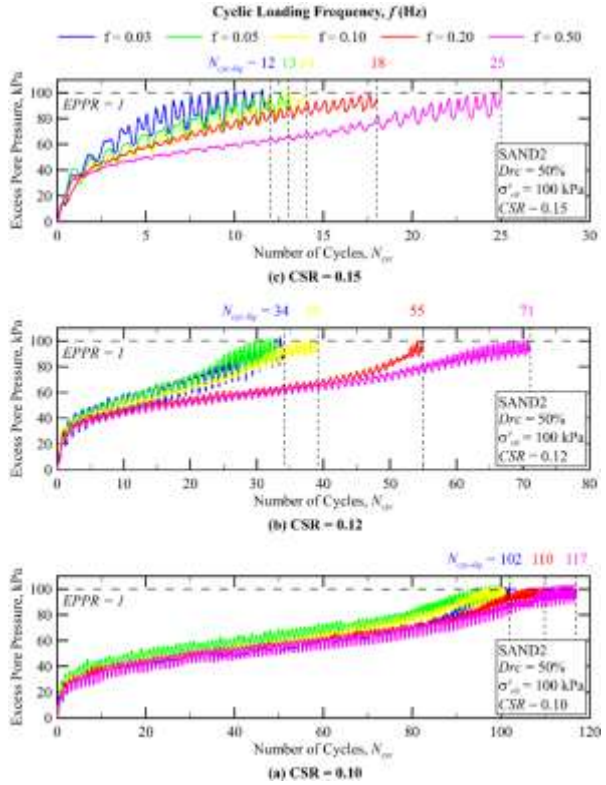

Fig. 9 Excess pore pressure generation versus number of cycles for the SAND2 sample under different loading frequencies: (a) CSR = 0.10, (b) CSR = 0.12, and (c) CSR = 0.15

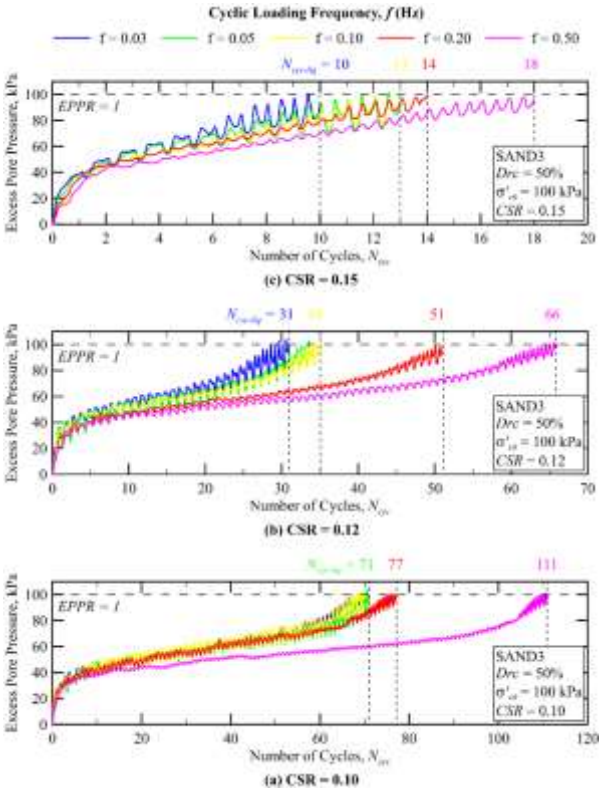

Fig. 10 Excess pore pressure generation versus number of cycles for the SAND3 sample under different loading frequencies: (a) CSR = 0.10, (b) CSR = 0.12, and (c) CSR = 0.15

SAND3 samples, respectively. Across all three sand types and CSR values, a consistent trend is observed: the number of cycles required to trigger initial liquefaction increases with increasing loading frequency.

As shown in Fig. 11(a), under a constant relative density of 50%, SAND1 exhibits a significant sensitivity to loading frequency. At a low CSR of 0.08, the number of cycles to liquefaction increases from 16–17 cycles at frequencies of 0.03–0.05 Hz to 72 cycles at 0.50 Hz. A similar trend is noted at CSR = 0.10, where $N_{cyc\text{-}liq}$ rises from 6–8 cycles (at low frequency) to 44 cycles at the highest frequency. These results indicate that SAND1 becomes increasingly resistant to liquefaction as the loading frequency increases. Fig. 11(b) illustrates the frequency-dependent behavior of SAND2. Under a moderate CSR of 0.10, the number of cycles remains relatively stable, ranging from 100 to 117 cycles across all frequencies, suggesting limited frequency influence at low cyclic stress. However, at higher CSR values (0.12 and 0.15), a more pronounced frequency effect is observed. For example, at CSR = 0.15, $N_{cyc\text{-}liq}$ increases from 12 cycles at 0.03 Hz to 25 cycles at 0.50 Hz. This indicates that as the cyclic demand increases, the role of loading frequency in influencing pore pressure generation and liquefaction resistance becomes more significant. Fig. 11(c) reveals a similar trend for SAND3. At the lowest CSR of 0.08, the increase in $N_{cyc\text{-}liq}$ with frequency is more subtle, rising from ~70 cycles at low frequencies to 111 cycles at 0.50 Hz. However, at higher CSR values (e.g., 0.15), the change becomes more distinct, with $N_{cyc\text{-}liq}$ increasing from 10 cycles at 0.03 Hz to 18 cycles at 0.50 Hz. These observations support the conclusion that higher loading frequencies slow the accumulation of excess pore pressure, thereby delaying the onset of liquefaction.

Across all sand types and CSR values, the results consistently demonstrate a nonlinear relationship between loading frequency and liquefaction resistance, which can be categorized into two distinct behavioral zones: Stable or Minor Effect Zone (f = 0.03–0.10 Hz) and Significant Increase Zone (f > 0.10 Hz). In the first Zone (Fig. 11), with the lower frequency range ($f \leq 0.10$ Hz), the number of cycles required to reach liquefaction remains relatively stable or increases only slightly. For example, in SAND1 under CSR = 0.08, $N_{cyc\text{-}liq}$ ranges narrowly from 16 to 19 cycles as frequency increases from 0.03 Hz to 0.10 Hz. A similar flat trend is observed in SAND2 and SAND3 across various CSR levels, where $N_{cyc\text{-}liq}$ remains almost unchanged within this frequency range. This behavior suggests that within this zone, excess pore pressure accumulates at a nearly constant rate, and loading frequency has minimal or negligible influence on the dynamic response of the soil.

In the second Zone (Fig. 11), When the frequency exceeds 0.10 Hz, a clear increase in $N_{cyc\text{-}liq}$ is observed, indicating that the soil becomes more resistant to liquefaction. For instance, in SAND1 at CSR = 0.08, $N_{cyc\text{-}liq}$ jumps from 19 cycles (at 0.10 Hz) to 52 and 72 cycles at 0.20 Hz and 0.50 Hz, respectively. Similar trends are

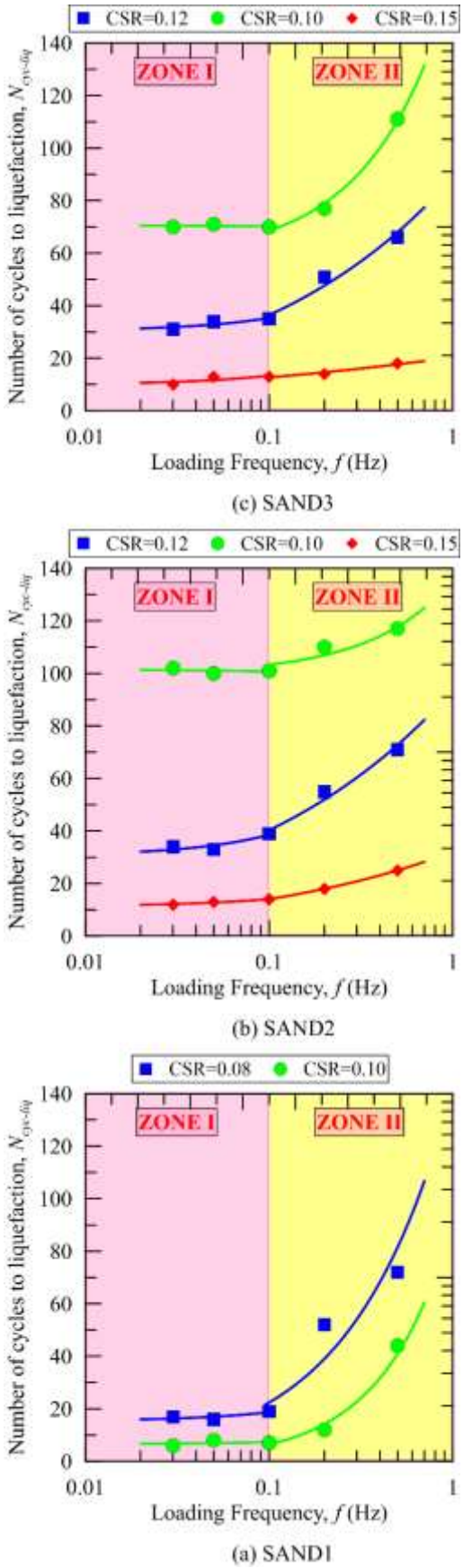

Fig. 11 Loading frequency versus number of cycles to liquefaction for (a) SAND1, (b) SAND2, and (c) SAND3 sample under different CSRs

evident in SAND2 and SAND3 for all CSR levels. This behavior reflects a reduction in the efficiency of pore pressure accumulation per cycle at higher frequencies, possibly due to reduced drainage time, particle rearrangement limitations, or incomplete stress transmission within short loading intervals.

The transition point between the two behavioral zones is consistently observed at approximately f = 0.10 Hz, regardless of the CSR value or sand type. This frequency thus appears to represent a critical or threshold frequency, separating stable/low-sensitivity behavior from a region where frequency exerts a strong influence on cyclic resistance. The consistency of this threshold across different materials and loading conditions suggests it may reflect a fundamental timescale governing pore pressure development in sandy soils under cyclic shear.

3.2 Effect of loading frequency on the liquefaction resistance of sand based on CRR_{15}

To further quantify the influence of loading frequency on liquefaction resistance, the cyclic resistance ratio corresponding to 15 cycles to liquefaction (CRR_{15}) was evaluated for each sand type under varying frequencies.

Figs. 12(a)-12(c) present the relationship between the cyclic stress ratio and the number of cycles to initial liquefaction for SAND1, SAND2, and SAND3, respectively, under various loading frequencies. As shown, each dataset exhibits a consistent nonlinear decay trend, indicating that higher CSRs lead to liquefaction within fewer cycles. These trends were fitted using the empirical power function proposed in previous studies (e.g., Boulanger and Idriss 2004, Park and Kim 2013), as expressed in Eq. (1)

$$CSR = a \times {N_{cyc-liq}}^{b} \quad (1)$$

where a and b are fitting parameters determined by regression analysis for each loading frequency and sand type. Based on these fitted curves, the cyclic resistance ratio corresponding to 15 cycles to liquefaction (CRR_{15}) was determined by substituting $N_{cyc\text{-}liq}$ = 15 into Eq. (1). This approach provides a consistent and comparative index of liquefaction resistance across different loading frequencies and soil types.

Table 3 summarizes the regression parameters (a, b) and corresponding CRR_{15} values obtained for each sand type (SAND1, SAND2, and SAND3) at different loading frequencies. These values were used to construct the frequency-dependent liquefaction resistance curves shown in Fig. 13.

As illustrated in Fig. 13, all three sand types exhibit a consistent trend: the CRR_{15} remains nearly constant or shows only a marginal increase within the frequency range of 0.03 to 0.10 Hz, which may be classified as a stable or minor-effect zone. For instance, CRR_{15} for SAND1 stays around 0.083–0.085 within this range, while SAND2 and SAND3 also show minimal variation (from 0.1427 to 0.1474 and 0.1382 to 0.1455, respectively). This suggests that, under low-frequency cyclic loading, the accumulation of excess pore pressure and the onset of liquefaction occur

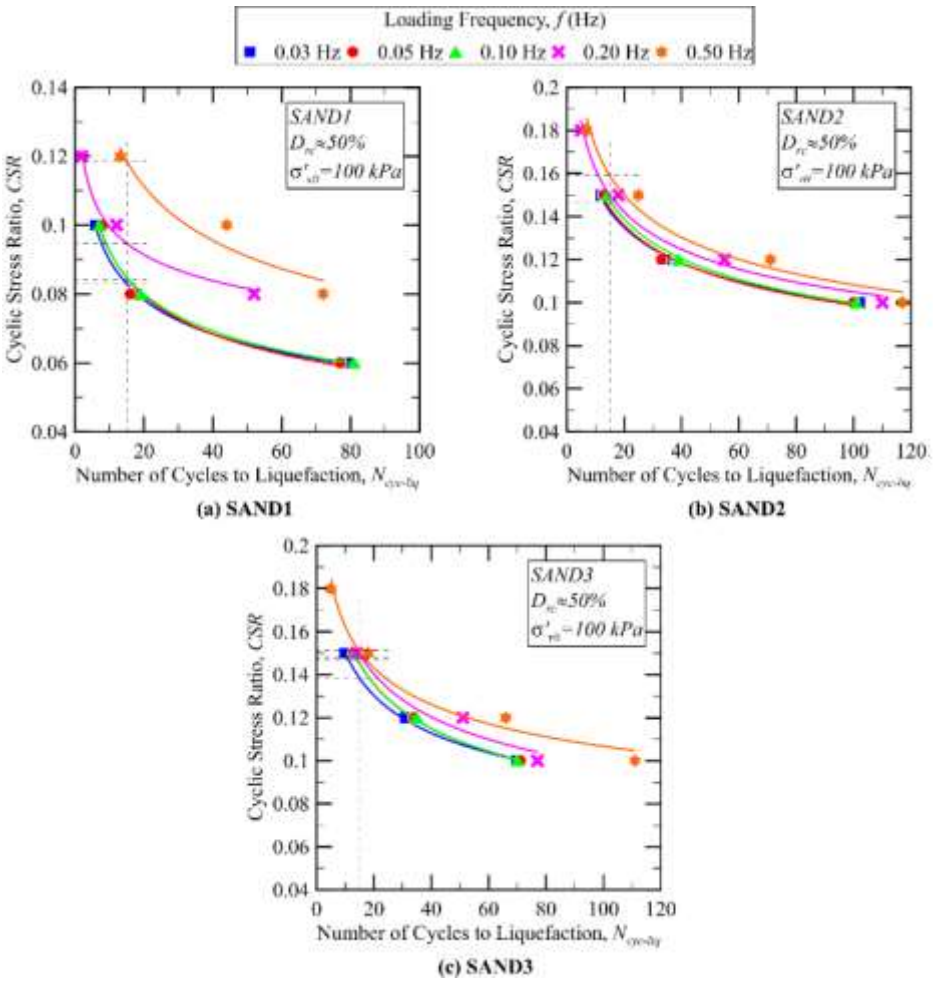

Fig. 12 The cyclic resistance curve of (a) SAND1, (b) SAND2, and (c) SAND3 with various loading frequency

Table 3 The cyclic resistance curve's parameters

Type	*f (Hz)*	*a*	*b*	CRR_{15}
SAND1	0.03	0.1415	-0.197	0.0830
	0.05	0.1529	-0.218	0.0850
	0.10	0.1490	-0.208	0.0850
	0.20	0.1323	-0.124	0.0950
	0.50	0.2152	-0.220	0.1190
SAND2	0.03	0.2380	-0.189	0.1427
	0.05	0.2456	-0.198	0.1437
	0.10	0.2568	-0.205	0.1474
	0.20	0.2498	-0.188	0.1501
	0.50	0.2753	-0.203	0.1589
SAND3	0.03	0.2428	-0.208	0.1382
	0.05	0.2771	-0.238	0.1455
	0.10	0.2786	-0.240	0.1455
	0.20	0.2730	-0.222	0.1496
	0.50	0.2471	-0.182	0.1509

in a similar manner, resulting in relatively unchanged liquefaction resistance.

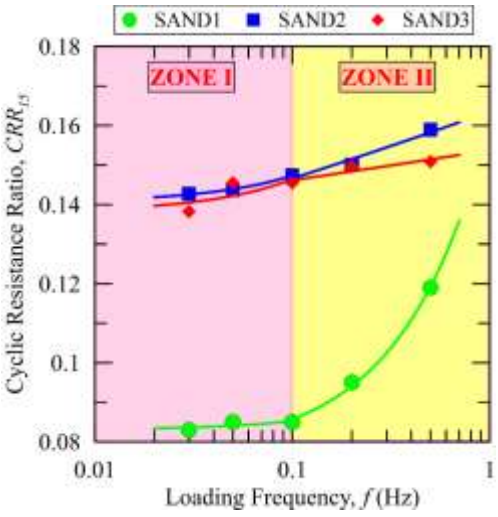

Fig. 13 Loading frequency versus cyclic resistance ratio

However, as the loading frequency increases beyond 0.10 Hz, a notable increase in CRR_{15} is observed. For example, the CRR_{15} of SAND1 increases from 0.085 at 0.10 Hz to 0.095 at 0.20 Hz, and further to 0.119 at 0.50 Hz. A similar rising pattern is seen in SAND2 (from 0.1474 to

0.1589) and SAND3 (from 0.1455 to 0.1509). This shift implies that higher frequencies demand a higher cyclic stress ratio to induce liquefaction within 15 cycles, reflecting an enhanced liquefaction resistance.

These findings clearly delineate two behavioral regimes: (i) Stable Zone ($f \leq 0.10$ Hz) where CRR_{15} remains nearly unchanged and (ii) Increasing Zone ($f > 0.10$ Hz) where CRR_{15} rises with frequency.

The threshold frequency of 0.10 Hz appears to represent a transitional boundary between these two regimes, which is consistent across all three soil types and CSR levels. This critical frequency likely marks a point beyond which the rate of pore pressure dissipation or particle rearrangement mechanisms are significantly influenced by the shortened time interval between successive loading cycles.

4. Conclusions

This study investigated the influence of loading frequency on the liquefaction resistance of three reconstituted sand samples (SAND1, SAND2, and SAND3) under undrained cyclic loading conditions. A series of cyclic direct simple shear (CDSS) tests were conducted across a range of cyclic stress ratios (CSRs) and loading frequencies varying from 0.03 Hz to 0.5 Hz. The objective was to evaluate how loading frequency affects the number of cycles to liquefaction ($N_{cyc\text{-}liq}$), the development of excess pore water pressure, and the cyclic resistance ratio at 15 cycles (CRR_{15}). The principal findings of this study are summarized as follows:

(i) All three sand types showed a consistent trend in pore pressure development under cyclic loading with different frequencies. A clear behavioral transition was observed at a frequency of approximately 0.10 Hz. Specifically, in the low-frequency range (0.03–0.10 Hz), changes in frequency had negligible to minor effects on the number of cycles to liquefaction. Conversely, when the loading frequency exceeded 0.10 Hz, a notable increase in $N_{cyc\text{-}liq}$ was observed, indicating enhanced resistance to liquefaction as loading frequency increased.

(ii) The CRR_{15} values remained relatively stable within the frequency range of 0.03 Hz to 0.10 Hz, but increased significantly for frequencies greater than 0.10 Hz. This observation further supports the existence of a transition frequency at $f = 0.10$ Hz, demarcating two behavioral regimes: a Stable or Minor-Effect Zone ($f \leq 0.10$ Hz) and an Increasing Resistance Zone ($f > 0.10$ Hz).

(iii) The threshold frequency of 0.10 Hz was consistently observed across all three sand types, regardless of CSR level. This reinforces the robustness of the identified transition point and its potential applicability as a critical frequency boundary in liquefaction assessment frameworks.

These findings highlight the significant role of loading frequency in the evaluation of liquefaction resistance. The experimental evidence presented here underscores the necessity of incorporating frequency effects into design considerations and predictive models, particularly for seismic loading scenarios where frequency content can vary widely.

Acknowledgments

The research described in this paper was financially supported by a National Research Foundation of Korea (NRF) grant funded by the Korean government (MSIT) (NRF-2021R1I1A3059731).

References

Amipour, S., Khashila, M., Bayoumi, A., Karray, M. and Chekired, M. (2022), "Specimens size effect D/H on cyclic behaviour and liquefaction potential of clean sand", *Acta Geotech.*, **17**(5), 2047-2057. https://doi.org/10.1007/s11440-021-01339-x.

Asadzadeh, M. and Soroush, A. (2017), "Macro- and micromechanical evaluation of cyclic simple shear test by discrete element method", *Particuology*, **31**, 129-139. https://doi.org/10.1016/j.partic.2016.05.015.

ASTM (2019), "Standard test method for consolidated undrained cyclic direct simple shear test under constant volume with load control or displacement control", ASTM D8296, ASTM International, West Conshohocken, PA, USA.

Bhattacharya, S., Tokimatsu, K., Goda, K., Sarkar, R., Shadlou, M. and Rouholamin, M. (2014), "Collapse of Showa Bridge during 1964 Niigata earthquake: A quantitative reappraisal on the failure mechanisms", *Soil Dyn. Earthq. Eng.*, **65**, 55-71. https://doi.org/10.1016/j.soildyn.2014.05.004.

Boulanger, R.W. and Idriss, I.M. (2004), *Evaluating the Potential for Liquefaction or Cyclic Failure of Silts and Clays*, Citeseer, Princeton, NJ, USA.

Boulanger, R.W. and Idriss, I.M. (2006), "Liquefaction susceptibility criteria for silts and clays", *J. Geotech. Geoenviron. Eng.*, **132**(11), 1413-1426. https://doi.org/10.1061/(ASCE)1090-0241(2006)132:11(1413).

Chang, N.Y., Hsieh, N.P., Samuelson, D.L. and Horita, M. (1982), "Effect of frequency on liquefaction potential of saturated Monterey No. O sand", *Comput. Method. Exp. Meas.*, Keramidas, G.A. and Brebbia, C.A. (Eds.), Springer, Berlin, Heidelberg, Germany, 433-446.

Chang, N.Y. and Ko, H.Y. (1982), "Effects of grain size distribution on dynamic properties and liquefaction potential of granular soils", *NASA STIRecon Tech. Rep. N*, **83**, 18966.

Coulter, H.W. and Migliaccio, R.R. (1966), *Effects of the Earthquake of March 27, 1964, at Valdez, Alaska*, U.S. Government Printing Office, Washington, D.C., USA.

Dash, H.K. and Sitharam, T.G. (2016), "Effect of frequency of cyclic loading on liquefaction and dynamic properties of saturated sand", *Int. J. Geotech. Eng.*, **10**(5), 487-492. https://doi.org/10.1080/19386362.2016.1171951.

Doherty, J. and Fahey, M. (2011), "Three-dimensional finite element analysis of the direct simple shear test", *Comput. Geotech.*, **38**(7), 917-924. https://doi.org/10.1016/j.compgeo.2011.05.005.

Dyvik, R., Berre, T., Lacasse, S. and Raadim, B. (1987), "Comparison of truly undrained and constant volume direct simple shear tests", *Géotechnique*, **37**(1), 3-10. https://doi.org/10.1680/geot.1987.37.1.3.

Hussain, M. and Sachan, A. (2019), "Effect of loading conditions and stress history on cyclic behavior of Kutch soil", *Geomech. Geoeng.*, **14**(3), 163-176. https://doi.org/10.1080/17486025.2019.1635716.

Kokusho, T. (2007), "Liquefaction strengths of poorly-graded and well-graded granular soils investigated by lab tests", *Earthq. Geotech. Eng. - Proc. 4th Int. Conf. Earthq. Geotech. Eng. - Invited Lectures*, Springer, 159-184.

Lee, K. and Fitton, J. (1969), "Factors affecting the cyclic loading

strength of soil", *Vibrations Effects of Earthquakes on Soils and Foundations*, ASTM International, West Conshohocken, PA, USA, 71-125.

Lee, K.L. and Focht, J.A. (1975), "Liquefaction potential at Ekotisk Tank in North Sea", *J. Geotech. Eng. Div.*, **101**(1), 1-18. https://doi.org/10.1061/AJGEB6.0000138.

Mohtar, C.E., Nakamura, Y. and Kwan, W.S. (2018), "Comparison of measured cyclic resistance of sand in simple shear tests under constant volume versus constant total vertical stress conditions", *Geotech. Earthq. Eng. Soil Dyn. V*, ASCE, Austin, TX, USA, 141-149.

Mulilis, J.P. (1975), "The effects of method of sample preparation on the cyclic stress-strain behaviour of sands", Technical Report, University of California, Berkeley, CA, USA.

Nong, Z., Park, S.S., Jeong, S.W. and Lee, D.E. (2020), "Effect of cyclic loading frequency on liquefaction prediction of sand", *Appl. Sci.*, **10**(13), 4520. https://doi.org/10.3390/app10134502.

Nong, Z.Z., Park, S.S. and Lee, D.E. (2021), "Comparison of sand liquefaction in cyclic triaxial and simple shear tests", *Soils Found.*, **61**(4), 1071-1085. https://doi.org/10.1016/j.sandf.2021.05.002.

NRC (1985), *Liquefaction of Soils during Earthquakes*, Committee on Earthquake Engineering, National Academy Press, Washington, D.C., USA.

Park, S.S. and Kim, Y.S. (2013), "Liquefaction resistance of sands containing plastic fines with different plasticity", *J. Geotech. Geoenviron. Eng.*, **139**(5), 825-830. https://doi.org/10.1061/(ASCE)GT.1943-5606.0000806.

Park, S.S. and Lee, D.E. (2024), "Effects of loading frequency and specimen size on the liquefaction resistance of clean sand", *Geomech. Eng.*, **37**(2), 123-135. https://doi.org/10.12989/gae.2024.37.2.123.

Park, S.S., Tran, D.K.L., Nguyen, T.N., Woo, S.W. and Sung, H.Y. (2023), "Effect of loading frequency on the liquefaction resistance of poorly graded sand", *Adv. Geospat. Technol. Min. Earth Sci. - Sel. Pap. 2nd Int. Conf. Geo-Spat. Technol. Earth Resour. 2022*, Springer, Singapore, 95-104.

Park, S.S., Woo, S.W., Nguyen, T.N. and Tran, D.K.L. (2024), "Effect of silt uniformity on the liquefaction resistance of sand–silt mixtures", *Soils Found.*, **64**(5), 101507. https://doi.org/10.1016/j.sandf.2024.101507.

Peacock, W.H. and Seed, H.B. (1968), "Sand liquefaction under cyclic loading simple shear conditions", *J. Soil Mech. Found. Div.*, **94**(3), 689-708. https://doi.org/10.1061/JSFEAQ.0001135.

Qin, Y. (2023), "Experimental investigation of liquefaction characteristics of saturated coral sand subjected to complex cyclic stress paths: Effects of loading frequency", *Appl. Ocean Res.*, **136**, 103573. https://doi.org/10.1016/j.apor.2023.103573.

Seed, H.B. (1979), "Soil liquefaction and cyclic mobility evaluation for level ground during earthquakes", *J. Geotech. Eng. Div.*, **105**(2), 201-255. https://doi.org/10.1061/AJGEB6.0000768.

Sonmezer, Y.B., Akyuz, A. and Kayabali, K. (2020), "Investigation of the effect of grain size on liquefaction potential of sands", *Geomech. Eng.*, **20**(3), 243-252. https://doi.org/10.12989/gae.2020.20.3.243.

Tatsuoka, F., Maeda, S., Fujii, S. and Yamada, S. (1983), "Cyclic undrained strengths of saturated sand under random and uniform loading and their relation", *Bull. Earthq. Res. Inst., Univ. Tokyo*, **16**, 11-31.

Tatsuoka, F., Toki, S., Miura, S., Kato, H., Okamoto, M., Yamada, S., Yasuda, S. and Tanizawa, F. (1986), "Some factors affecting cyclic undrained triaxial strength of sand", *Soils Found.*, **26**(3), 99-116. https://doi.org/10.3208/sandf1972.26.99.

Tran, D.K.L., Woo, S.W., Hwang, K.B. and Park, S.S. (2024a), "Effect of lateral confinement method on excess pore pressure generation under strain-controlled cyclic direct simple shear test", *Jpn. Geotech. Soc. Spec. Publ.*, **10**(17), 570-575. https://doi.org/10.3208/jgssp.v10.OS-6-04.

Tran, D.K.L., Woo, S.W., Lee, S.D., Nguyen, N.N. and Park, S.S. (2024b), "Couple effect of loading frequency and uniformity coefficient on the liquefaction resistance of sand", *Proc. 3rd Int. Conf. Sustain. Civ. Eng. Archit.*, Lecture Notes in Civil Engineering, (Eds., Reddy, J.N., Wang, C.M., Luong, V.H. and Le, A.T.), Springer, Singapore, 1085-1091.

Vaid, Y.P., Fisher, J.M., Kuerbis, R.H. and Negussey, D. (1990), "Particle gradation and liquefaction", *J. Geotech. Eng.*, **116**(4), 698-703. https://doi.org/10.1061/(ASCE)0733-9410(1990)116:4(698).

Vaid, Y.P. and Sivathayalan, S. (2000), "Fundamental factors affecting liquefaction susceptibility of sands", *Can. Geotech. J.*, **37**(3), 592-606. https://doi.org/10.1139/t00-040.

Vernese, F.J. and Lee, K.L. (1977), *Effect of Frictionless Caps and Bases in the Cyclic Triaxial Test*, U.S. Army Corps of Engineers, Waterways Experiment Station, Vicksburg, MS, USA.

Wong, R.T., Seed, H.B. and Chan, C.K. (1975), "Cyclic loading liquefaction of gravelly soils", *J. Geotech. Eng. Div.*, **101**(6), 571-583. https://doi.org/10.1061/AJGEB6.0000174.

Wood, F.M., Yamamuro, J.A. and Lade, P.V. (2008), "Effect of depositional method on the undrained response of silty sand", *Can. Geotech. J.*, **45**(11), 1525-1537. https://doi.org/10.1139/T08-079.

Yamamuro, J.A. and Monkul, M.M. (2010), "Influence of densification method on some aspects of undrained behaviour", *Proceedings of the Int. Conf. Recent Adv. Geotech. Earthq. Eng. Soil Dyn.*, San Diego, CA, USA, 1-8.

Yoshimi, Y. and Oh-oka, H. (1975), "Influence of degree of shear stress reversal on the liquefaction potential of saturated sand", *Soils Found.*, **15**(3), 27-40. https://doi.org/10.3208/sandf1972.15.27.

Youd, T.L., Idriss, I.M., Andrus, R.D., Arango, I., Castro, G., Christian, J.T., Dobry, R., Finn, W.D.L., Harder, L.F., Hynes, M.E., Ishihara, K., Koester, J.P., Liao, S.S.C., Marcuson, W.F., Martin, G.R., Mitchell, J.K., Moriwaki, Y., Power, M.S., Robertson, P.K., Seed, R.B. and Stokoe, K.H. (2001), "Liquefaction resistance of soils: Summary report from the 1996 NCEER and 1998 NCEER/NSF workshops on evaluation of liquefaction resistance of soils", *J. Geotech. Geoenviron. Eng.*, **127**(10), 817-833. https://doi.org/10.1061/(ASCE)1090-0241(2001)127:10(817).

Yue, C., Xu, C., Liang, K. and Xiuli, D. (2023), "Effect of cyclic loading frequency on cyclic behaviour of saturated sand", *Soil Dyn. Earthq. Eng.*, **173**, 108095. https://doi.org/10.1016/j.soildyn.2023.108095.

Zhou, R. (2025), "Experimental analysis on the cyclic strength and deformation characteristics of marine coral sand under different loading frequencies", *Soil Dyn. Earthq. Eng.*, **184**, 109225. https://doi.org/10.1016/j.soildyn.2025.109225.

Zhu, Z., Zhang, F., Peng, Q., Dupla, J.C., Canou, J., Cumunel, G. and Foerster, E. (2021), "Effect of the loading frequency on the sand liquefaction behaviour in cyclic triaxial tests", *Soil Dyn. Earthq. Eng.*, **147**, 106779. https://doi.org/10.1016/j.soildyn.2021.106779.

Zuo, K., Gu, X., Liu, H., Hu, J. and Gao, G. (2023), "Influences of particle size distribution and fines content on the excess pore water pressure generation of sand-silt mixtures under cyclic loading", *Soil Dyn. Earthq. Eng.*, **174**, 108201. https://doi.org/10.1016/j.soildyn.2023.108201.

CC